Increased crevassing across accelerating Greenland Ice Sheet margins

Thomas R. Chudley
Department of Geography, Durham University, Durham, UK
https://orcid.org/0000-0001-8547-1132

Ian M. Howat
Byrd Polar and Climate Research Center, Ohio State University, Columbus, OH, USA
School of Earth Sciences, Ohio State University, Columbus, OH, USA
https://orcid.org/0000-0002-8072-6260

Michalea D. King
Polar Science Center, University of Washington, Seattle, WA, USA
https://orcid.org/0000-0002-8138-4362

Emma J. MacKie
Department of Geological Sciences,
University of Florida, Gainesville, FL, USA
https://orcid.org/0000-0002-6303-5249

Correspondence: Tom Chudley (thomas.r.chudley@durham.ac.uk)

Increased crevassing across accelerating Greenland Ice Sheet margins

Thomas R. Chudley[1,2], Ian M. Howat[2,3], Michalea D. King[4], Emma J. MacKie[5]

[1] Department of Geography, Durham University, Durham, UK

5   [2] Byrd Polar and Climate Research Center, Ohio State University, OH, USA

[3] School of Earth Sciences, Ohio State University, OH, USA

[4] Polar Science Center, University of Washington, WA, USA

[5] Department of Geological Sciences, University of Florida, FL, USA

Correspondence: Tom Chudley (thomas.r.chudley@durham.ac.uk)

10   ## Abstract

Surface crevassing on the Greenland Ice Sheet is a large source of uncertainty in processes controlling mass loss, including calving, ice rheology, and water routing. However, no work has comprehensively mapped the location of surface crevasses or examined their evolution through time. Here, we use high-resolution digital elevation

15   models to map the 3-dimensional volume of crevasse fields across the Greenland Ice Sheet in 2016 and 2021. Parallelling prior observations of Greenland discharge, the change in the total ice-sheet-wide volume of crevasses between these two years was within measurement error (+4.3 ± 5.9%), masking large and significant increases at accelerating marine-terminating sectors of the ice sheet (up to +25.3 ± 10.1% in the

20   Southeast sector). These sectoral increases were offset only by a reduction in crevasse volume in the central west sector (-14.2 ± 3.2%), particularly at Sermeq Kujalleq (Jakobshavn Isbræ), which underwent a temporary slowdown over the study period. Changes in crevasse volume correlate strongly with antecedent discharge changes, indicating that Greenland's acceleration forces significant increases in crevassing on a

25   timescale of less than five years. This response provides a mechanism for mass-loss-promoting feedbacks on sub-decadal timescales, including increased calving, faster flow, and accelerated water transfer to the bed.

Main

Surface crevasses result from spatial and temporal ice flow variability and, thus, are

30   ubiquitous across the complex, fast-flowing margins of the Greenland Ice Sheet (GrIS).

Crevasses exert a first-order control on varied glaciological processes: fractures can act as pre-existing weaknesses that can promote calving and instability at glacier fronts [1], whilst accumulated damage can soften the large-scale rheology of ice [2]. As key hydrological pathways [3–5], crevasses transfer up to half of Greenland's seasonal surface runoff to the

35 bed [6]. This transport can alter ice rheology by increasing ice temperature [7], modify the pressure of the subglacial hydrological system [4,5,8,9], and promote basal melt [10]. By modulating the rate of meltwater transport to the ocean, further influence is exerted on terminus melt, fjord circulation, and fjord biogeochemistry [11–13]. These crevasse-dependent processes hold the potential to induce significant feedbacks between ice flow acceleration

40 and mass loss [4,14], making them a key source of uncertainty in projections of future Greenland Ice Sheet behaviour [1,15].

Given these mass-loss-accelerating feedbacks, it is critical to understand how crevasse fields are changing across Greenland. It is expected that increases in crevasse extent are common across the ice sheet due to a (i) increasing tensile stresses resulting from a

45 steepening ablation area and outlet glacier acceleration [14], and (ii) an increase in meltwater available for hydrofracture [9]. Only one multitemporal study exists, which observed an increase crevasse extent across a region of West Greenland between 1985 and 2009 [4]. However, observations of surging glaciers have shown that crevasse fields can propagate on much faster timescales (months - years) in response to rapid dynamic

50 change [16,17]. Outlet glaciers around the GrIS are exhibiting accelerations of the same magnitude and rate as glacier surges [18–20], suggesting that recent accelerations could initiate crevasse growth and subsequent feedbacks over sub-decadal timescales. However, no study has yet monitored short-term change in crevassing in Greenland, nor conducted a comprehensive assessment across the full ice sheet.

55 Recognition of crevassing's importance has motivated improved observation and modelling capabilities. Studies have shown that simple parameterisations used in modelling studies are not a good predictor of crevasse distribution [3,21] due to mixed-mode fracture formation [22], variable ice rheology [23], and the advection of crevasses from zones of active opening [24]. Therefore, improved observations are required to develop and

60 validate models of fracture formation and propagation [25] and parameterise their behaviour in models of ice sheet dynamics and hydrology [6,26]. Optical satellite observation methods have progressed from manual delineation [4] to computer vision [27,28] and machine learning [29,30] approaches. However, these are limited to assessing crevasse presence without critical information about crevasse depth, and attempts to map geometry have thus far

65   been limited to profiles [21]. Recent public availability of comprehensive, multitemporal, and high-resolution digital elevation models (DEMs) of the polar regions [31] provide an unprecedented opportunity to assess 3-D crevasse geometry and evolution at high spatial and temporal resolution. Here, we use these data to present the first three-dimensional record of crevassing over the entire GrIS in 2016 and 2021, across a period of time with

70   significant dynamic accelerations [18–20] and decelerations [32]. We use these maps to quantify the rate and extent of regional trends in crevassing and provide the first ice-sheet-wide observational evidence of the relationship between crevassing and ice dynamic change.

Multitemporal Greenland-wide crevasse inventories

75
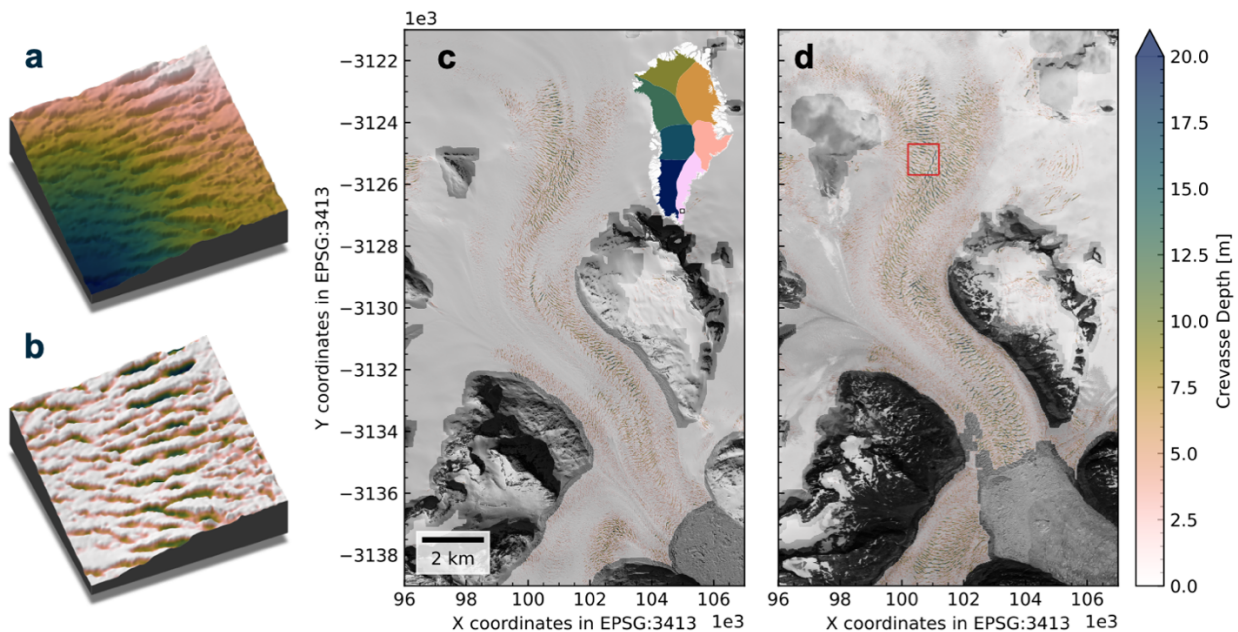
Figure 1: Examples of crevasse field extraction and evolution from ArcticDEM strips. (a) A 500 × 500 m ArcticDEM sample of a crevassed surface. (b) Sample following crevasse extraction, with a colour scale matching panels c and d. (c) Crevasse depths at the head of Anorituup Kangerlua fjord from a 2016-04-13 ArcticDEM strip, overlaid onto a contemporaneous Worldview-1

80   *image. (d) Same as (c), but for 2021-07-15 after sustained acceleration and retreat. Red box identifies regions of panels a and b. Inset: location of Anorituup Kangerlua fjord (white box) within Greenland, with sectors in Figs. 2 and 3 coloured separately.*
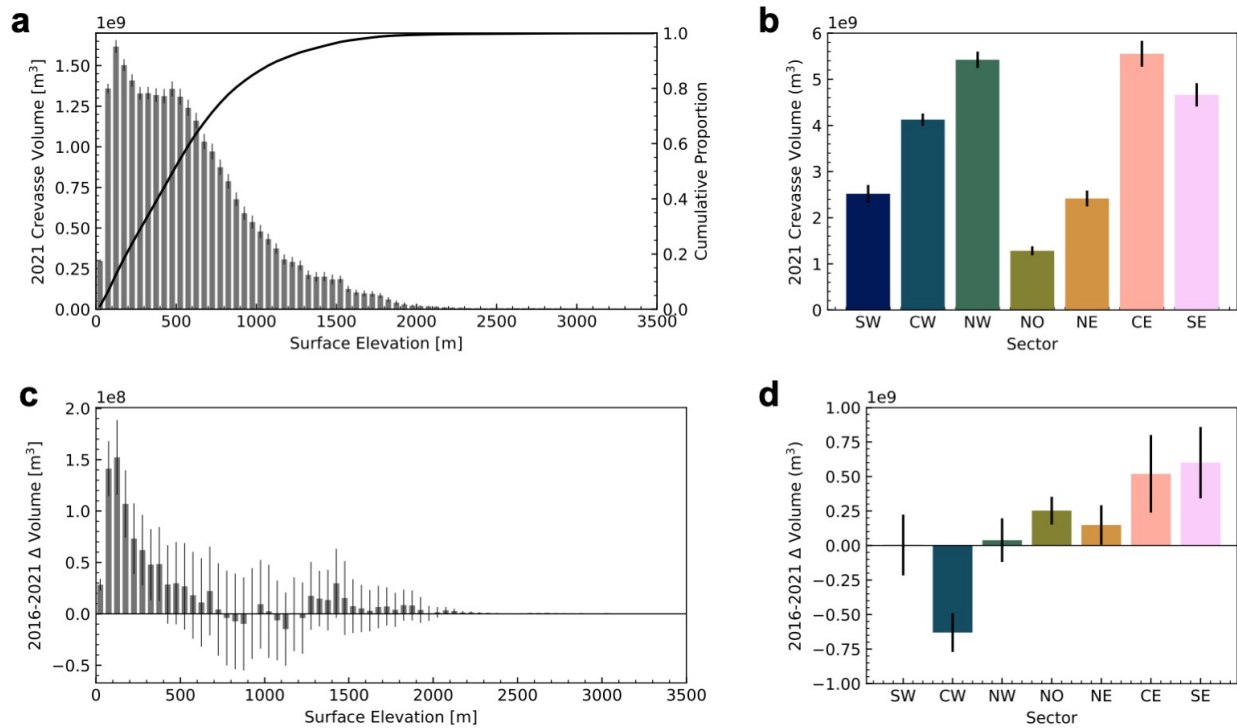
Figure 2: Crevasse volume and changes across the ice sheet. *(a) Histogram of 2021 crevasse volume with surface elevation across the ice sheet. (b) Bar chart of 2021 crevasse volume per sector. (c) Histogram of 2016-2021 crevasse volume change with surface elevation across the ice sheet. (d) Bar chart of 2016-2021 crevasse volume change per sector. Error bars represent 2σ measurement uncertainties (see methods). A version of Figure 2d with the ice-sheet-wide value presented for scale is included as Supplementary Fig. 1.*

We extracted crevasse depth from 2 m resolution ArcticDEM strips [31] across the GrIS in 2016 and 2021 (Fig. 1; Methods). We integrated pixel-based crevasse depth to estimate the air-filled crevasse volume, providing the first estimates of crevasse inventory and change at an ice sheet, sector, and basin scale.

In 2021, we mapped an estimated $25.98 \times 10^9 \pm 1.30 \times 10^9$ m³ of crevasse volume across ~89% of the melt zone (see Methods) of the GrIS. Crevasse distribution overwhelmingly dominated low elevations near the ice margin (Fig. 2a), with 68% of crevasse volume concentrated below 700 m above mean sea level (AMSL), and 95% below 1420 m AMSL. However, crevasses were less present at the lowest elevations, below 100 m AMSL (Fig. 2a), mostly due to the height of marine-terminating ice cliffs [33]. Hence, beneath 100 m ice either does not exist (it has already calved) or is land-terminating without significant crevassing. Significant sectoral variation was observed (Fig. 2b), with high volumes of crevasses in the CE, NW, SE, and CW sectors (typified by large, fast-flowing, marine outlets), and lower volumes in the land-terminating SW and less-dynamic NO and NE sectors. The crevasse elevation distribution was also highly variable

between sectors (Extended Data Fig. 1). Sector NW exhibited a sharp elevation gradient in crevasse volumes, up to 1000 m AMSL, whilst the similarly marine-terminating SE and CE sectors had longer-tailed distributions up to 2000 m AMSL. This reflects the typical long trunks of SE/CE sectors, which extended diffusive acceleration from the ice front along their length, whilst NW glaciers are closely linked to the surrounding ice sheet with strongly convergent flow until close to the glacier margins [34,35]. Sector NO and NE are characterised by a low-elevation bias, with little crevassing above 150 m. This likely reflects the predominance of crevassing on floating ice tongues concentrated in these sectors [36]. Finally, the unique distribution of sector CW, with the bulk of crevassing between the 200-800 m AMSL elevation bands, reflects the dominance of large marine-terminating outlets with short trunks and high calving fronts such as Sermeq Kujalleq (Jakobshavn Isbræ) (hereafter SKJI).

The change in crevasse volume from 2016 and 2021 across the Greenland Ice Sheet was within measurement uncertainty, with a total change in crevasse volume of $+9.32 \times 10^8 \pm 13.01 \times 10^8$ m^3 (+4.3 ± 5.9%). However, this total masks spatially heterogeneous behaviour by elevation and sector. Beneath 400 m AMSL, crevasse volume increased significantly across all elevations, peaking at 100-150 m AMSL (Fig. 2c). Beneath ~100 m AMSL, increased crevassing was offset by a loss of surface area as marine-terminating glaciers retreated. Changes were highly heterogeneous at a sectoral level (Fig. 2d), varying between +25.3 ± 10.1% (NO) to -14.2 ± -3.2% (CW). No significant changes were observed in the NW , nor the land-terminating SW, whilst significant increases in the NO, NE, CE, and SE were offset by a large reduction in the volume of crevasses in the CW sector (fig. b). Sectors displayed distinct elevation distributions (Extended Data Fig. 2). In the NO and NE, increases were limited to ice tongues at the lowest elevations (<~400 m AMSL), whilst increases in the CE and SE were distributed more evenly across the lowest ~1000 m AMSL due to diffusive thinning along the trunk.

Relationship to dynamics

Changes in crevasse morphology and extent reflect changes in ice dynamics: specifically, the surface stress regime [1,37,38]. We used records of total ice flux through outlet glacier termini, termed discharge, as a proxy for the bulk dynamic change of ice sectors and basins. Specifically, we compared annual crevasse volume (2021) to the mean discharge of the preceding five years (2017-2021), assuming that total crevasse volume in any individual year is the cumulative product of stresses integrated over multiple years (see

Methods). This proposed relationship between antecedent discharge and crevasse volume
140   holds at a sectoral scale in our dataset (Fig. 3a; p = 0.04). Sectors predominantly
comprised of slow-flowing, land-terminating margins (SW), or less dynamic, well-
buttressed outlet glaciers (NO/NE) exhibited low crevasse volumes compared to sectors
with high numbers of fast-flowing marine-terminating outlets (SE/CE/NW/CW).
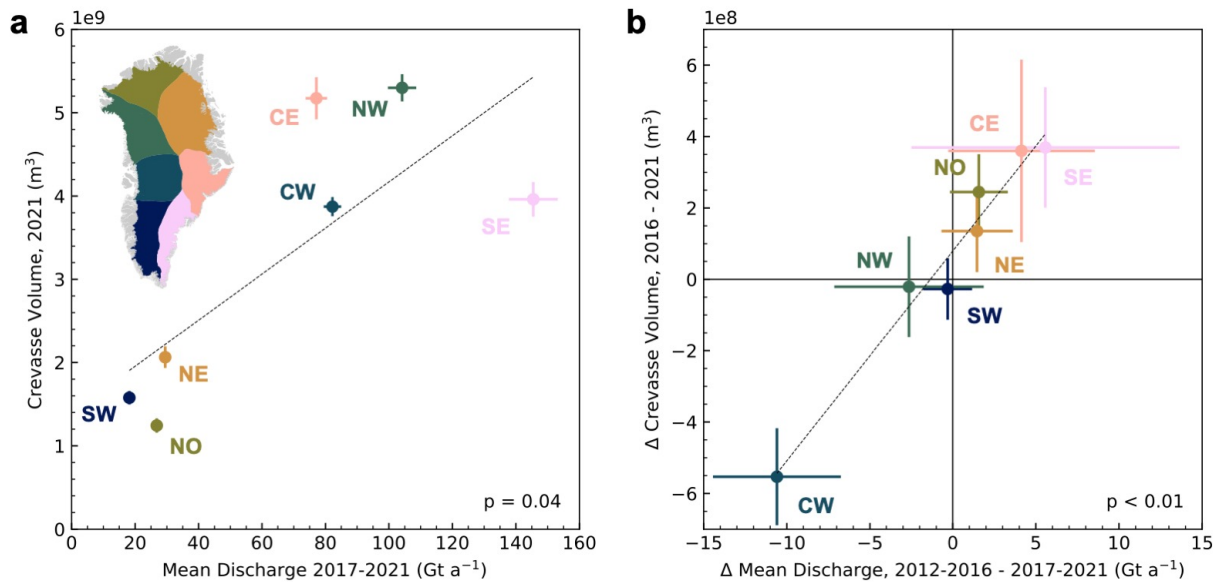
145   ***Figure 3: Sectoral-scale discharge comparison.*** *(a) Scatter plot showing sectoral-scale*
relationships between 2017-2021 mean annual discharge and 2021 crevasse volume. Error bars
represent 2σ uncertainties. (b) Scatter plot showing sectoral-scale relationship between change in
mean annual discharge between the 2011-2016 and 2017-2021 periods and change in crevasse
volume between 2016-2021. Error bars represent 2σ uncertainties. Note that only drainage basins
150   *with >60% crevasse observations and valid discharge records are included in the sectoral sum*
totals. Full regression results are presented in Supplementary Table 1.

We found a striking, sector-scale relationship (fig. 3b; p < 0.01) between the change in
crevasse volumes between 2016-2021 and the change in the corresponding antecedent
five-year mean discharge (between 2012-2016 and 2017-2021), consistent with the
155   hypothesis that changes in crevasse volume and extent are forced by changes in the
dynamic regime of glaciers. Indeed, our large-scale crevasse observations closely parallel
the Greenland discharge literature: both quantities are observed to exhibit
insignificant/stable changes at an ice-sheet-scale in the latter half of the 2010s, but this net
figure masks significant inter-sectoral variation [39,40]. In particular, increases at eastern
160   marine-terminating sectors are balanced by well-documented reductions in discharge from
the CW sector in the second half of the 2010s [40], mirroring the similar sectoral imbalance
in crevasse volume change. This is largely driven by SKJI, which has exhibited significant

slowdown since 2014 following a reduction in ocean forcing [32,41]. Meanwhile, increased crevassing across the CE and SE sectors were consistent with accelerating ice velocities and discharge observed at both glacier and sectoral levels, linked to warming air and ocean temperatures [18,19,42,43].

We further assessed crevasse volume and changes at a basin level (Fig. 4a-b). This analysis confirmed a significant positive relationship (p < 0.01) between discharge and crevasse volume (Fig. 4c). This relationship exhibits a higher variability than the sectoral scale. We suggest that this relationship is again analogous to the Greenland discharge literature, whereby large-scale forcing is modulated by glacier-specific factors including, among others, fjord and glacier geometry [44]. In our case, local factors modulating the relationship between discharge and crevasse expression may include ice rheology (ice temperature, pre-existing damage, etc), the specific distribution of stresses (e.g. plug flow concentrating high surface stresses into shear margins), and other factors including ice velocity, thickness, and basal traction.
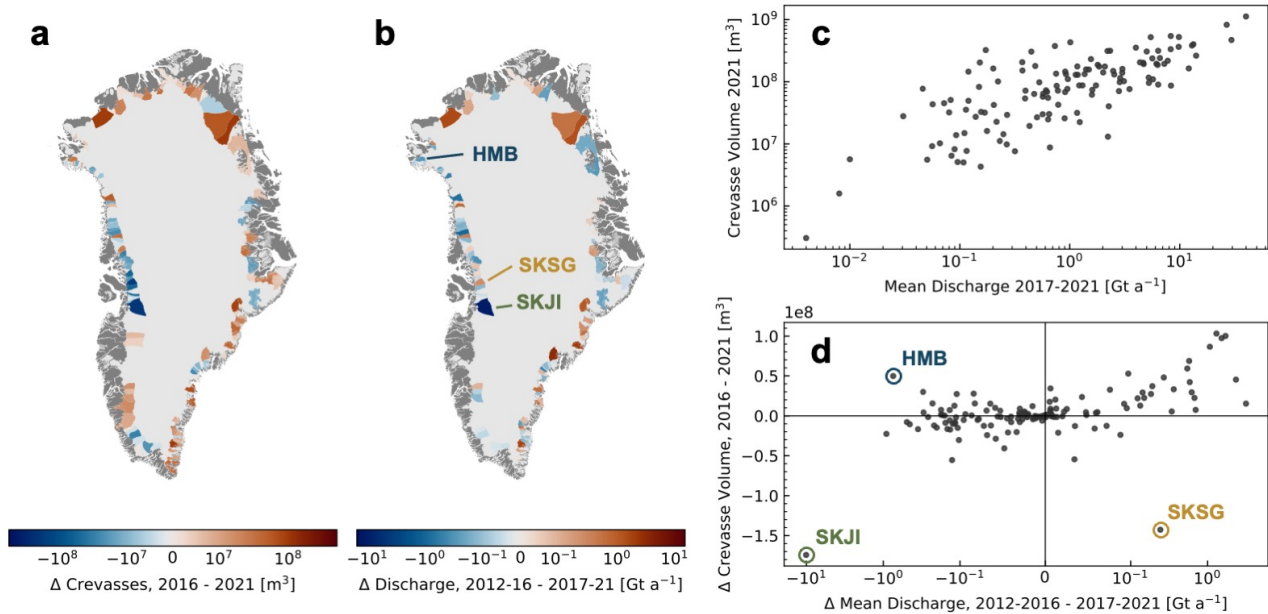
Figure 4: Basin-scale discharge comparison. *(a) Change in crevasse volume between 2016-2021 at a basins with significant (>60%) map coverage. (b) Change in mean annual discharge between the 2011-2016 and 2017-2021 periods. (c) Basin-scale relationship between 2017-2021 mean annual discharge and 2021 crevasse volume. (d) Basin-scale relationship between change in mean annual discharge between the 2011-2016 and 2017-2021 periods and change in crevasse volume between 2016-2021. Outliers Harald Moltke Bræ (HMB), Sermeq Kujalleq (Jakobshavn Isbræ; SKJI), and Sermeq Kujalleq (Store Glacier; SKSG) are labelled. Only basins of a total area > 100 km² are shown.*

More nuance is revealed in the relationship between change in discharge and change in crevassing (Fig. 4d). Although there was a significant relationship between an increase in discharge and an increase in crevassing ($p < 0.01$ where Δ discharge > 0), there appeared to be a weaker relationship between crevassing and a decrease in discharge: in fact, the only glacier to display a significant reduction in both discharge and crevassing was SKJI. After excluding SKJI, the relationship was not significant ($p = 0.44$ where Δ discharge < 0). We suggest this could relate to differing timescales required to open and close crevasse fields, consistent with previous work that has concluded that crevasse formation outpaces crevasses closure [37,45]. Opening of crevasse fields likely occurs rapidly (< five years), forced by the higher tensile surface stresses occurring alongside ice acceleration. However, an equivalent reduction in velocity at outlet glaciers does not necessitate a compressive stress regime that would actively close crevasses. Instead, the closure of crevasse fields requires the generational replacement of individual crevasses within a field by smaller crevasses formed under lower-tensile-stress conditions. As such, any reduction in crevasse field volume is rate-limited by surface velocity. The reduction in crevasse volume shown here at SKJI (labelled in Fig. 4d) may be an instructive exception, demonstrating how the fast-flowing regime propagated crevasse closure within a five-year timescale. Alternatively, the rapid collapse in velocities at SKJI after 2016 [32] could have induced a sufficiently large regions of compression to actively close crevasses on a short timescale. Whilst our work supports previous field observations that crevasse response to dynamics operate over multi-annual timescales [45], the basin and sectoral-scale heterogeneity observed here suggests that further work is necessary to understand response time variability and its controls.

Further individual basin-level anomalies also provide insights into crevasse behaviours. For instance, Harald Moltke Bræ (HMB in Fig. 4d) showed distinct reduction in discharge yet an increase in crevassing. This was an aliasing effect related to the surge occurring 2013-2019 [46], which resulted in an increase in (relict) crevasses between 2016 and 2021 even as the discharge reduced. Sermeq Kujalleq (Store Glacier) (SKSG hereafter and in Fig. 4d) exhibits the opposite anomaly, undergoing significant decreases in crevasse volume despite an increase in discharge. We hypothesise that this may relate to rapid summer deceleration events that occurred in 2018 and 2019 (Supplementary Fig. 2). SKSG consistently displays these behaviours, likely associated with instabilities in basal hydrology and sliding . However, the deceleration events in these two summers were particularly extreme, with velocity collapsing by as much as 50% in 2019 (Supplementary Fig. 2). The resulting perturbation to the glacier strain field may have contributed to a

reduced crevasse volume. If these seasonal deceleration events were contributory factors, the magnitude and variability of deceleration events may have an outsized impact on crevasse evolution in glaciers that exhibit this behaviour.

Implications

225   We provide the first, Greenland-wide observations of crevasse volume and distribution, revealing significant changes in crevassing from 2016 to 2021 (sectoral-scale variation from -14.2% to +25.3%) that correlate with the dynamic evolution of marine-terminating outlets. Although total change (+4.3 ± 5.9%) is within measurement uncertainty, significant sector-scale increases in crevassing occur in most sectors (Fig. 2d), offset by the CW

230   sector – in particular SKJI, which is known to have undergone a significant slowdown between 2016-2019 [32]. Recent data indicate that SKJI is once again exhibiting acceleration and associated dynamic thinning [49], suggesting that SKJI will no longer offset Greenland-wide increases in crevassing over the next several years. The five-year time step assessed here provides evidence of crevasse response time to dynamic changes in

235   Greenland an order-of-magnitude faster than previously identified by satellite observation [4]. However, it is apparent that crevasse fields responded to dynamic events on a range of multi-annual timescales – in particular, slower responses where glaciers slowed – and further work should attempt to better clarify this response rate.

The ability to observe crevasses in 3-D provides a major advance over two-dimensional

240   mapping from imagery alone [27,28]. We have observed significant increases in crevasse volume in pre-existing crevasse fields at low elevations (marine-terminating outlets). This change, not previously able to be assessed, highlights a pathway for externally forced (ocean- or atmosphere-driven) dynamic accelerations to generate a number of positive feedbacks to ice loss to through increased crevassing [37]. Increased damage over annual

245   timescales can act to weaken shear margins [2]. By transferring water to the bed [4,6,26], crevasses induce rheological changes [7,14], modify basal friction [4], and – upon reaching the ocean – amplify submarine melting at the terminus [13]. Finally, crevasses advected to the calving front play a role in accelerating glacier calving [1,50]. The ice-sheet-wide methods, datasets, and behaviours presented here provide a starting point to properly calibrate and

250   validate damage representation in large-scale dynamic models, accommodating the effects of ice damage and crevassing into predictions of future ice sheet behaviour.

References

1. Berg, B. & Bassis, J. Crevasse advection increases glacier calving. *Journal of Glaciology* **68**, 977–986 (2022).

2. Lhermitte, S. *et al.* Damage accelerates ice shelf instability and mass loss in Amundsen Sea Embayment. *Proceedings of the National Academy of Sciences* **117**, 24735–24741 (2020).

3. Chudley, T. R. *et al.* Controls on Water Storage and Drainage in Crevasses on the Greenland Ice Sheet. *Journal of Geophysical Research: Earth Surface* **126**, e2021JF006287 (2021).

4. Colgan, W. *et al.* An increase in crevasse extent, West Greenland: Hydrologic implications. *Geophysical Research Letters* **38**, (2011).

5. McGrath, D., Colgan, W., Steffen, K., Lauffenburger, P. & Balog, J. Assessing the summer water budget of a moulin basin in the Sermeq Avannarleq ablation region, Greenland ice sheet. *Journal of Glaciology* **57**, 954–964 (2011).

6. Koziol, C., Arnold, N., Pope, A. & Colgan, W. Quantifying supraglacial meltwater pathways in the Paakitsoq region, West Greenland. *Journal of Glaciology* 1–13 (2017) doi:10.1017/jog.2017.5.

7. Lüthi, M. P. *et al.* Heat sources within the Greenland Ice Sheet: dissipation, temperate paleo-firn and cryo-hydrologic warming. *The Cryosphere* (2015) doi:10.5194/tc-9-245-2015.

8. Cavanagh, J. P., Lampkin, D. J. & Moon, T. Seasonal Variability in Regional Ice Flow Due to Meltwater Injection Into the Shear Margins of Jakobshavn Isbræ. *Journal of Geophysical Research: Earth Surface* **122**, 2488–2505 (2017).

9. Lampkin, D. J., Amador, N., Parizek, B. R., Farness, K. & Jezek, K. Drainage from water-filled crevasses along the margins of Jakobshavn Isbræ: A potential catalyst for catchment expansion. *Journal of Geophysical Research: Earth Surface* **118**, 795–813 (2013).

10. Young, T. J. *et al.* Rapid basal melting of the Greenland Ice Sheet from surface meltwater drainage. *Proceedings of the National Academy of Sciences* **119**, e2116036119 (2022).

11. Cowton, T., Slater, D., Sole, A., Goldberg, D. & Nienow, P. Modeling the impact of glacial runoff on fjord circulation and submarine melt rate using a new subgrid-scale parameterization for glacial plumes. *Journal of Geophysical Research: Oceans* **120**, 796–812 (2015).

12. Kanna, N. *et al.* Meltwater Discharge From Marine-Terminating Glaciers Drives Biogeochemical Conditions in a Greenlandic Fjord. *Global Biogeochemical Cycles* **36**, e2022GB007411 (2022).

13. Slater, D. A. & Straneo, F. Submarine melting of glaciers in Greenland amplified by atmospheric warming. *Nat. Geosci.* 1–6 (2022) doi:10.1038/s41561-022-01035-9.

14. Colgan, W., Sommers, A., Rajaram, H., Abdalati, W. & Frahm, J. Considering thermal-viscous collapse of the Greenland ice sheet. *Earth's Future* **3**, 252–267 (2015).

15. Alley, R. B. *et al.* Iceberg Calving: Regimes and Transitions. *Annual Review of Earth and Planetary Sciences* **51**, 189–215 (2023).

16. Herzfeld, U. C. & Mayer, H. Surge of Bering Glacier and Bagley Ice Field, Alaska: an update to August 1995 and an interpretation of brittle-deformation patterns. *Journal of Glaciology* **43**, 427–434 (1997).

17. Trantow, T. & Herzfeld, U. C. Crevasses as Indicators of Surge Dynamics in the Bering Bagley Glacier System, Alaska: Numerical Experiments and Comparison to Image Data Analysis. *Journal of Geophysical Research: Earth Surface* **123**, 1615–1637 (2018).

18. Bevan, S. L., Luckman, A. J., Benn, D. I., Cowton, T. & Todd, J. Impact of warming shelf waters on ice mélange and terminus retreat at a large SE Greenland glacier. *The Cryosphere* **13**, 2303–2315 (2019).

19. Chudley, T. R., Howat, I. M., King, M. D. & Negrete, A. Atlantic water intrusion triggers rapid retreat and regime change at previously stable Greenland glacier. *Nat Commun* **14**, 2151 (2023).

20. Williams, J. J., Gourmelen, N. & Nienow, P. Complex multi-decadal ice dynamical change inland of marine-terminating glaciers on the Greenland Ice Sheet. *Journal of Glaciology* 1–14 (2021) doi:10.1017/jog.2021.31.

21. Enderlin, E. M. & Bartholomaus, T. C. Sharp contrasts in observed and modeled crevasse patterns at Greenland's marine terminating glaciers. *The Cryosphere* **14**, 4121–4133 (2020).

22. van der Veen, C. J. Crevasses on glaciers. *Polar Geography* **23**, 213–245 (1999).

23. Campbell, S. *et al.* Strain-rate estimates for crevasse formation at an alpine ice divide: Mount Hunter, Alaska. *Annals of Glaciology* **54**, 200–208 (2013).

24. Mottram, R. H. & Benn, D. I. Testing crevasse-depth models: a field study at Breiðamerkurjökull, Iceland. *Journal of Glaciology* **55**, 746–752 (2009).

25. Albrecht, T. & Levermann, A. Fracture field for large-scale ice dynamics. *Journal of Glaciology* **58**, 165–176 (2012).

26. Clason, C. C. *et al.* Modelling the transfer of supraglacial meltwater to the bed of Leverett Glacier, Southwest Greenland. *The Cryosphere* **9**, 123–138 (2015).

27. Izeboud, M. & Lhermitte, S. Damage detection on antarctic ice shelves using the normalised radon transform. *Remote Sensing of Environment* **284**, 113359 (2023).

28. Van Wyk de Vries, M., Lea, J. M. & Ashmore, D. W. Crevasse density, orientation and temporal variability at Narsap Sermia, Greenland. *Journal of Glaciology* 1–13 (2023) doi:10.1017/jog.2023.3.

29. Lai, C.-Y. *et al.* Vulnerability of Antarctica's ice shelves to meltwater-driven fracture. *Nature* **584**, 574–578 (2020).

30. Surawy-Stepney, T., Hogg, A. E., Cornford, S. L. & Hogg, D. C. Mapping Antarctic crevasses and their evolution with deep learning applied to satellite radar imagery. *The Cryosphere* **17**, 4421–4445 (2023).

31. Porter, C. *et al.* ArcticDEM - Strips, Version 4.1. Harvard Dataverse https://doi.org/10.7910/DVN/C98DVS (2022).

32. Khazendar, A. *et al.* Interruption of two decades of Jakobshavn Isbrae acceleration and thinning as regional ocean cools. *Nat. Geosci.* **12**, 277–283 (2019).

33. Parizek, B. R. *et al.* Ice-cliff failure via retrogressive slumping. *Geology* **47**, 449–452 (2019).

34. Howat, I. M., Joughin, I. & Scambos, T. A. Rapid Changes in Ice Discharge from Greenland Outlet Glaciers. *Science* **315**, 1559–1561 (2007).

325 35. Moon, T., Joughin, I., Smith, B. & Howat, I. 21st-century evolution of Greenland outlet glacier velocities. *Science* **336**, 576–578 (2012).

36. Reeh, N. Greenland Ice Shelves and Ice Tongues. in *Arctic Ice Shelves and Ice Islands* (eds. Copland, L. & Mueller, D.) 75–106 (Springer Netherlands, Dordrecht, 2017). doi:10.1007/978-94-024-1101-0_4.

37. Colgan, W. *et al.* Glacier crevasses: Observations, models, and mass balance implications. *Reviews of* 330 *Geophysics* **54**, 119–161 (2016).

38. van der Veen, C. J. Fracture mechanics approach to penetration of surface crevasses on glaciers. *Cold Regions Science and Technology* **27**, 31–47 (1998).

39. King, M. D. *et al.* Dynamic ice loss from the Greenland Ice Sheet driven by sustained glacier retreat. *Commun Earth Environ* **1**, 1–7 (2020).

335 40. Mankoff, K. D. *et al.* Greenland Ice Sheet solid ice discharge from 1986 through March 2020. *Earth System Science Data* **12**, 1367–1383 (2020).

41. Joughin, I., Shean, D. E., Smith, B. E. & Floricioiu, D. A decade of variability on Jakobshavn Isbræ: ocean temperatures pace speed through influence on mélange rigidity. *The Cryosphere* **14**, 211–227 (2020).

340 42. Black, T. E. & Joughin, I. Multi-decadal retreat of marine-terminating outlet glaciers in northwest and central-west Greenland. *The Cryosphere* **16**, 807–824 (2022).

43. Liu, J., Enderlin, E., Marshall, H.-P. & Khalil, A. Synchronous retreat of southeast Greenland's peripheral glaciers. *Geophysical Research Letters* **49**, e2022GL097756 (2022).

44. Wood, M. *et al.* Ocean forcing drives glacier retreat in Greenland. *Science Advances* **7**, eaba7282 345 (2021).

45. Harper, J. T., Humphrey, N. F. & Pfeffer, W. T. Crevasse patterns and the strain-rate tensor: a high-resolution comparison. *Journal of Glaciology* **44**, 68–76 (1998).

46. Müller, L. *et al.* Surges of Harald Moltke Bræ, north-western Greenland: seasonal modulation and initiation at the terminus. *The Cryosphere* **15**, 3355–3375 (2021).

350 47. Moon, T. *et al.* Distinct patterns of seasonal Greenland glacier velocity. *Geophys Res Lett* **41**, 7209–7216 (2014).

48. Vijay, S. *et al.* Greenland ice-sheet wide glacier classification based on two distinct seasonal ice velocity behaviors. *J Glaciol* 1–8 (2021) doi:10.1017/jog.2021.89.

49. Khan, S. A. *et al.* Greenland Mass Trends From Airborne and Satellite Altimetry During 2011–2020. 355 *Journal of Geophysical Research: Earth Surface* **127**, e2021JF006505 (2022).

50. Krug, J., Weiss, J., Gagliardini, O. & Durand, G. Combining damage and fracture mechanics to model calving. *The Cryosphere* **8**, 2101–2117 (2014).

Methods

Crevasse Detection

Crevasse depth detection from ArcticDEM strips

360 We mapped crevasses using 2-m resolution ArcticDEM v4.1 strips [31] provided by the Polar Geospatial Center (PGC). The method, which we make public as a Python package and associated Jupyter Notebooks (https://github.com/trchudley/crevdem), will also work on other 2 m strips provided by the PGC as part of the REMA [51] or EarthDEM [52] projects,

365 although we cannot guarantee the optimal length scale we determine here is representative of other sectors of the Cryosphere. We first preprocessed the strips by filtering them only to good-quality ice surfaces. This was done by filtering strips to 'good' data as indicated by the PGC-provided bitmasks; filtering out bedrock using the Greenland Ice Mapping Project (GrIMP) Ice and Ocean classification mask [53]; and geoid-correcting

370 the heights to mean sea level using the EIGEN-6C4 geoid model [54] provided within BedMachine v4 [55]. Finally, when over 1 km^2 of strip area is < 10 m above mean sea level (AMSL), we applied a routine to filter out 'marine surfaces' (ocean, sea ice, and low-lying ice mélange) following a previously published iceberg detection routine [56]. In this approach, we constructed a histogram of elevation in 0.25 m bins between -15 and +15 m

375 AMSL, and identified contemporaneous sea level as the modal bin. We assigned all regions beneath 10 m of our determined contemporaneous sea level as marine surfaces, leaving only terrestrial ice and floating ice tongues.

After pre-processing, we determined the observed open-air crevasse depth, which we define here as the difference between the raw DEM height and a nominal 'filled crevasse'

380 surface. We first detrended the DEM using a large Gaussian filter (standard deviation 200 m), before applying a black top hat (BTH) filter to the detrended surface to determine the negative deviation from the local maxima [57]. Gaussian and BTH filters were both applied using OpenCV implementations [58]. The diameter of the BTH kernel was set to be 60 m, following spatial variogram analysis of crevassed surfaces around Greenland (see section

385 'Determining the optimal crevasse length scale'). Following previous approaches [57], we identify pixels as 'crevassed' where the BTH-filtered value is greater than a threshold value, here > 1 m. To generate a nominal 'crevasse-filled' surface, we further remove the crevassed pixels and filled the surfaces using an inverse-distance weighting algorithm as implemented in GDAL [59], followed by two 3×3 averaging filter smoothing operations to

390   dampen artefacts. Crevasse depth was determined as the difference between the interpolated 'surface' and the crevasse bottom in the raw DEM.

Determining the optimal crevasse length scale

To determine the kernel size, we assessed the typical crevasse length scale by modelling the spatial covariance, or variogram, which quantifies the variance of spatial

395   measurements as a function of their separation distance [60]. The variogram was used to determine the range, or separation distance at which measurements are spatially uncorrelated. This parameter has previously been used to determine the optimal kernel size for BTH filtering of DEMs [57]. To find a representative range parameter, we estimated the ranges at four different glaciers covering a range of sectors and dynamic contexts:

400   Sermeq Kujalleq (Jakobshavn Isbræ), Sermeq Kujalleq (Store Glacier), KJV Steenstrups Nordre Bræ, and Isunnguata Sermia. We manually identified five 1500 × 1500 m sample zones, which we subjectively ranked on an ordinal scale of 'crevasse intensity' from 0 (no crevasses) to 4 (most crevassed region of glacier). We then constructed spatial variograms of the five sample zones using SciKit-GStat [61]. We use DEMs from 2021

405   (Supplementary Fig. 3a-d), which we detrended as described above, randomly sampling 2% of the pixels within the sample zone to increase computational efficiency. To estimate the representative crevasse width, we used the range of the variograms estimated using a Gaussian variogram model, which best fit our experimental variograms. The mean estimated spatial range of the most crevassed sample regions (crevasse intensity = 4) was

410   62.4 m; the mean estimated spatial of the top two most crevassed regions (crevasse intensity ≥ 3) was 57.3 m (Supplementary Fig. 3a-d). We selected 60 m as a representative range (and thus kernel size) to apply to fast-flowing regions of the Greenland Ice Sheet.

Ice-sheet wide processing and mosaicking

415   We produced GrIS-wide maps of crevasses in 2016 and 2021, years when ArcticDEM strip coverage was high and particularly conducive to comprehensive assessment.

To eliminate extraneous processing in the ice interior, we generously defined an AOI mask as anywhere melt occurs in the RACMO2.3p2 1 km melt model between 2016 and 2021 [62], dilated by 10 km. We took all strips intersecting this region between April and October

420   with a reported RMSE < 2 m and a component image baseline < 60 minutes. In total, we processed 4667 strips in 2016 and 4207 strips in 2021 (Supplementary Table 2), with a subsequent coverage of our AOI of 75% and 86% respectively (Supplementary Fig. 4). We

note that coverage is biased towards outlet glaciers and no-data regions are commonly high-elevation, low-velocity sectors in the accumulation zone. This benefits our assessment as no-data regions are largely regions without crevassing present.

Due to the advection of individual crevasses, 2 m resolution crevasse depth maps cannot be directly compared. Instead, we enabled comparison between 2016 and 2021 by summing crevasse depth maps into 200 m resolution crevasse volume maps, which we refer to as the 'exposed crevasse air volume'. To obtain a single annual mosaic, we found the median value of all overlapping strips where multiple exist. All crevasse volumes discussed in this study have been aggregated into established sectors and basins [63]. However, for the interested reader, we present samples of changes at select basins at native resolution, alongside contemporaneous changes in the MEaSUREs Greenland annual ice sheet velocity mosaics [64,65], in the supplementary material (Supplementary Figs. 5a-f).

Uncertainty and Method Intercomparison

We assigned a measurement uncertainty to our aggregate crevasse volume measurements by assessing variation in contemporaneous strip measurements. To do this, we assessed variance within the Nioghalvfjerdsfjorden (79˚N) discharge basin in 2021, which we selected due to its high overlapping strip records (up to 21 overlapping strips) and large variation in surface types. Across all valid pixels within the 79˚N area of interest, we calculate the per-pixel standard deviation in crevasse depth values across the basin. The mean standard deviation value across the 200 m grid cells was 407 m^3 (10,175 m^3 km^{-2}). We apply this per-pixel uncertainty value to all basins, and present measurement uncertainty as 2σ error bars within the figures presented in this paper.

As a first-order comparison against alternative crevasse detection methods, we compare our method to contemporaneous crevasse datasets at a previously studied crevasse field (70.5399°, -50.1423°) located at Store Glacier in 2018. Here, there exists UAV-derived 15-cm-resolution map of crevasses (dated 2018-07-08) classified using object-based machine learning techniques [3]. We compare this against a Sentinel-2-derived map of crevasses using a Gabor filter approach [28] for the date 2018-07-02, and apply our current approach on an ArcticDEM strip dated 2018-06-24. Data is shown in Supplementary Figs. 6 and 7. Our method represents an advance on these previous approaches as it provides a direct measure of crevasse depth rather than simply area. Whilst this also means the workflows are not quantiatively comparable (see 'Limitations' section), overall there is good

qualitative agreement between the methods. Individual crevasses are identifiable between the three datasets. In comparison to the Sentinel-2 approach, our method is sensitive to smaller crevasses, as well as less likely to misclassify the edges of snow/ice boundaries. These advantages are balanced by the much higher temporal resolution of the Sentinel-2

460   stack, which can detect sub-seasonal changes [28]. Using the UAV data as ground validation, we assess the limit of crevasse width detectable by our method to be approximately 10 m. This matches the previous assessment made using a more rudimentary ArcticDEM segmentation approach [3].

Limitations

465   The limitations of our dataset are derived from the resolution and optical source data of the raw ArcticDEM strips.

First, the 2 m resolution of the source strips places a fundamental lower bound on the minimum identifiable crevasse diameter. In practice, comparison with UAV data has shown that a realistic minimum diameter observable with these methods is ~10 m (see section

470   "Uncertainty and Method Intercomparison"). Although this limits applications for smaller inland crevasses, it is more than sufficient for observation of changes at crevasse fields in fast-flowing (>100 m/a) regions, where the crevasse width averages ~60 m (see section 'Determining the optimal crevasse length scale').

Second, the reported crevasse depth values produced by our method are commonly in the

475   range of 10-100 m deep. This does not represent full crevasse depth, as even crevasses with surface expressions of only 10s of centimetres have been shown reach depths of hundreds of metres [66]. However, larger crevasses of the type observed in this study (~10s metres in width) have been observed to be consistently infilled with debris in high-resolution UAV-derived datasets [67], limiting the observed depth in optically-derived DEMs.

480   As such, we refer to the volumetric measurements in this study as the 'exposed crevasse air volume', acknowledging that full-depth measurements are not possible. Full crevasse depths have extrapolated from simpler 2D profiles in the past [21], suggesting that a similar method to extrapolate 3D datasets may be possible in the future.

Third, the optical nature of the source data meant that we cannot extract snow-filled

485   crevasses that may be possible to detect using other methods, such as SAR or GPR [68]. However, the large diameters of crevasses detected here are highly unlikely to fill with snow: in analysis of Sentinel-2 optical imagery with a similar effective resolution for crevasse detection, crevasse density was not observed to change over a seasonal cycle

or in an indicative elevation-dependent way that suggested snowfill [28]. The month filtering,

490   ablation zone masking, and median mosaicking we performed during the mosaicking

process mean we consider it very unlikely that snowfill can explain any of the large-scale

multitemporal change we observe in our study. Any small-scale variation should be

adequately captured in our uncertainty assessment, alongside other minor sources of

measurement variance (e.g. satellite geometry).

495   Fourth, by selecting a relatively shallow BTH threshold of 1 m, we implicitly included

features that are not true crevasses (e.g. shallow ditches and river gulleys). We chose to

do this as we are interested in volumetric change rather than area change, and these

shallow features do not represent significant contributions to aggregate volume

measurements. Increasing the BTH threshold to a higher value introduces a much larger

500   volume of false negatives instead of a small volume of false positives. Experimentation

showed that increasing the threshold for crevasse identification may aesthetically improve

the binary crevasse mask, but resulted in an increased variance in our volumetric

uncertainty measurements as legitimate crevasses began to be inconsistently masked

from DEM strips. As a result, we do not recommend our method for crevasse area

505   segmentation tasks. Other methods have previously been proposed for this task using

ArcticDEM [3].

Finally, our analysis covers only the years 2016 and 2021, rather than a continuous

dataset over the study period. Due to limitations of data coverage in the ArcticDEM strip

dataset, it is not possible to achieve satisfactory coverage of other years at a Greenland

510   scale. We make the assumption that crevasses represent the 'damped' expression of

multi-annual ice dynamics, and so assessing change between these years is valid as there

is a negligible chance that changes we detect may be a result of capturing high interannual

variability or measurement error. To show this, we extract 2016-2021 annual crevasse

volume at six select Greenlandic outlets where data availability is sufficient: three where

515   significant acceleration occurs over the time period (Anorituup Kangerlua fjord, KIV

Steenstrups, and Kjer Glacier); and three where stable or decelerating trends are

prevalent (Umiammakku Sermiat, Store Glacier, and Rink Isbræ) (Supplementary Fig. 2).

We overlay ice velocity from ITS_LIVE data, and, for Anorituup Kangerlua fjord, also

present individual mosaics for further reference (Supplementary Fig. 8). These data

520   support our assumption that interannual variation is low and dynamic response occurs on

time-scales greater than one year (e.g. KIV Steenstrups and Kjer glaciers both continue to

increase in volume in 2021 despite peaking in velocity in 2020), and aligns with previous

studies on this topic 45,69. Additionally, the secular trends in crevasse volume are clearly associated with a parallel increases and/or decreases in glacier velocity. This supports our

525 inference that significant changes are attributable to real and significant changes in crevasse volume rather than short-term variability or measurement error.

Discharge

We compared crevasse change to discharge change as a proxy for the bulk dynamic change of ice sectors and basins. This assumes that the time-evolving discharge, ice

530 velocity, and the magnitude/extent of extensional stress are broadly correlated at a basin and sectoral scale. Further, as discharge is a function of both ice velocity and outlet size, comparing bulk crevasse volume to bulk discharge implicitly controlled for available ice surface area, unlike direct measurements of ice flow velocity or strain rates.

Changes in dynamic forcing takes time to propagate through to observed changes in

535 crevasse fields, as crevasses are the cumulative product of opening and closing stresses integrated over time. Over the majority of the ice sheet, these strain rates are of the order of 0.01 a^{-1} of less[70], hence changes in crevasse width cannot fluctuate more than a few percent in a given year and changes will be dominated by multi-year trends in flow. This is evidenced by low inter-annual trends and long-term secular trends on the order of years

540 observed in prior studies [28,30]. A period of 5 years was selected to be a reasonable estimate of crevasse response time in line with published estimates of crevasse lifecycles in studies of valley glaciers [45,69] and ensured discharge records do not overlap. As a result, we compared the average annual discharge for the preceding five years (2012-2016 for the 2016 crevasse dataset and 2017-2021 for the 2021 dataset).

545 We obtained 2012-2021 monthly ice discharge measurements from flux gate measurements at marine-terminating glaciers from two complimentary datasets [39,40] (hereafter the 'King' and 'Mankoff' datasets). Each individual dataset covers specific outlet glaciers, and neither is comprehensive across all Greenland outlets. As the pre-defined drainage basins [63] frequently contain multiple outlets, any individual drainage basin may

550 be comprehensively covered by flux gates from either the King or Mankoff datasets, both, or neither. As a result, we combined the datasets to cover as many discharge basins as possible. Of the 254 basins in the dataset, we assessed 192 as having discharge records in at least one dataset. Of these, 185 basins were usable. 138 had outlets comprehensively covered by both King and Mankoff, so we took the average of the two

555 datasets. 29 and 16 basins were comprehensively covered only by King or Mankoff

respectively. At two basins, unusually, the two datasets covered mutually exclusive outlets within the basin, and we used the sum of the two datasets to represent full basin discharge.

Data Availability

560 Source data (necessary to reproduce this study and the figures within (Greenland-wide crevasse volume rasters, and basin-scale aggregations of crevasse volume and discharge) have been deposited in a Figshare repository available at https://doi.org/10.6084/m9.figshare.23937654 [prior to publication, this can be accessed at https://figshare.com/s/3085649423185efbe4d0]. ArcticDEM 2 m strips are available

565 at https://doi.org/10.7910/DVN/OHHUKH. The EIGEN-6C4 model is available as part of the BedMachine v4 at https://doi.org/10.5067/VLJ5YXKCNGXO. The GrIMP ice and ocean classification mask is available at https://doi.org/10.5067/B8X58MQBFUPA. Raw Mankoff discharge data is available at https://doi.org/10.22008/promice/data/ice_discharge.

Code Availability

570 The full workflow to download and extract crevasses from ArcticDEM and REMA imagery is publicly available as a Python package at https://github.com/trchudley/crevdem.

Methods References

51. Howat, I. M. *et al.* The Reference Elevation Model of Antarctica - Strips, Version 4.1. Harvard Dataverse https://doi.org/10.7910/DVN/X7NDNY (2022).

575 52. Porter, C. *et al.* EarthDEM - Strips, Version 1. Harvard Dataverse https://doi.org/10.7910/DVN/LHE9O7 (2022).

53. Howat, I. M., Negrete, A. & Smith, B. E. The Greenland Ice Mapping Project (GIMP) land classification and surface elevation data sets. *The Cryosphere* **8**, 1509–1518 (2014).

54. Förste, C. *et al.* EIGEN-6C4 The latest combined global gravity field model including GOCE data up to

580 degree and order 2190 of GFZ Potsdam and GRGS Toulouse. 55102156 Bytes, 3 Files GFZ Data Services https://doi.org/10.5880/ICGEM.2015.1 (2014).

55. Morlighem, M. *et al.* BedMachine v3: Complete Bed Topography and Ocean Bathymetry Mapping of Greenland From Multibeam Echo Sounding Combined With Mass Conservation. *Geophys. Res. Lett.* 2017GL074954 (2017) doi:10.1002/2017GL074954.

585 56. Shiggins, C. J., Lea, J. M. & Brough, S. Automated ArcticDEM iceberg detection tool: insights into area and volume distributions, and their potential application to satellite imagery and modelling of glacier–iceberg–ocean systems. *The Cryosphere* **17**, 15–32 (2023).

57. Kodde, M. P., Pfeifer, N., Gorte, B. G. H., Geist, T. & Höfle, B. Automatic glacier surface analysis from airborne laser scanning. *International Archives of the Photogrammetry, Remote Sensing and Spatial* 590 *Information Sciences* **36**, 221–226 (2007).

58. Bradski, G. The OpenCV Library. Dr. Dobb's Journal: Software Tools for the Professional Programmer **25**, 120–123 (2000).

59. Rouault, E. *et al.* GDAL. Zenodo https://doi.org/10.5281/ZENODO.5884351 (2023).

60. Matheron, G. Principles of geostatistics. *Economic Geology* **58**, 1246–1266 (1963).

595 61. Mälicke, M. SciKit-GStat 1.0: a SciPy-flavored geostatistical variogram estimation toolbox written in Python. *Geoscientific Model Development* **15**, 2505–2532 (2022).

62. Noël, B., van de Berg, W. J., Lhermitte, S. & van den Broeke, M. R. Rapid ablation zone expansion amplifies north Greenland mass loss. *Science Advances* **5**, eaaw0123 (2019).

63. Mouginot, J. & Rignot, E. Glacier catchments/basins for the Greenland Ice Sheet. 4137543 bytes Dryad 600 https://doi.org/10.7280/D1WT11 (2019).

64. Joughin, I. MEaSUREs Greenland Ice Velocity Annual Mosaics from SAR and Landsat, Version 5. NASA National Snow and Ice Data Center DAAC https://doi.org/10.5067/USBL3Z8KF9C3 (2023).

65. Joughin, I., Smith, B. E., Howat, I. M., Scambos, T. & Moon, T. Greenland flow variability from ice-sheet-wide velocity mapping. *Journal of Glaciology* **56**, 415–430 (2010).

605 66. Hubbard, B. *et al.* Borehole-Based Characterization of Deep Mixed-Mode Crevasses at a Greenlandic Outlet Glacier. *AGU Advances* **2**, e2020AV000291 (2021).

67. Chudley, T. R., Christoffersen, P., Doyle, S. H., Abellan, A. & Snooke, N. High-accuracy UAV photogrammetry of ice sheet dynamics with no ground control. *The Cryosphere* **13**, 955–968 (2019).

68. Thompson, S. S. *et al.* Comparing satellite and helicopter-based methods for observing crevasses, 610 application in East Antarctica. *Cold Regions Science and Technology* **178**, 103128 (2020).

69. Meier, M. F. The mechanics of crevasse formation. *Internat. Assoc. Scientific Hydrology* **46**, 500–508 (1958).

70. Cuffey, K. M. & Paterson, W. S. B. *The Physics of Glaciers*. (Academic Press, 2010).

Corresponding Author

615 Correspondence and requests for materials should be addressed to Tom Chudley,
thomas.r.chudley@durham.ac.uk

Acknowledgements

Author contributions

TRC: Conceptualisation, methodology, software, formal analysis, investigation, writing – original draft, writing – review & editing, visualisation, funding acquisition.

IMH: Conceptualisation, methodology, writing – review & editing, supervision, project administration, funding acquisition.
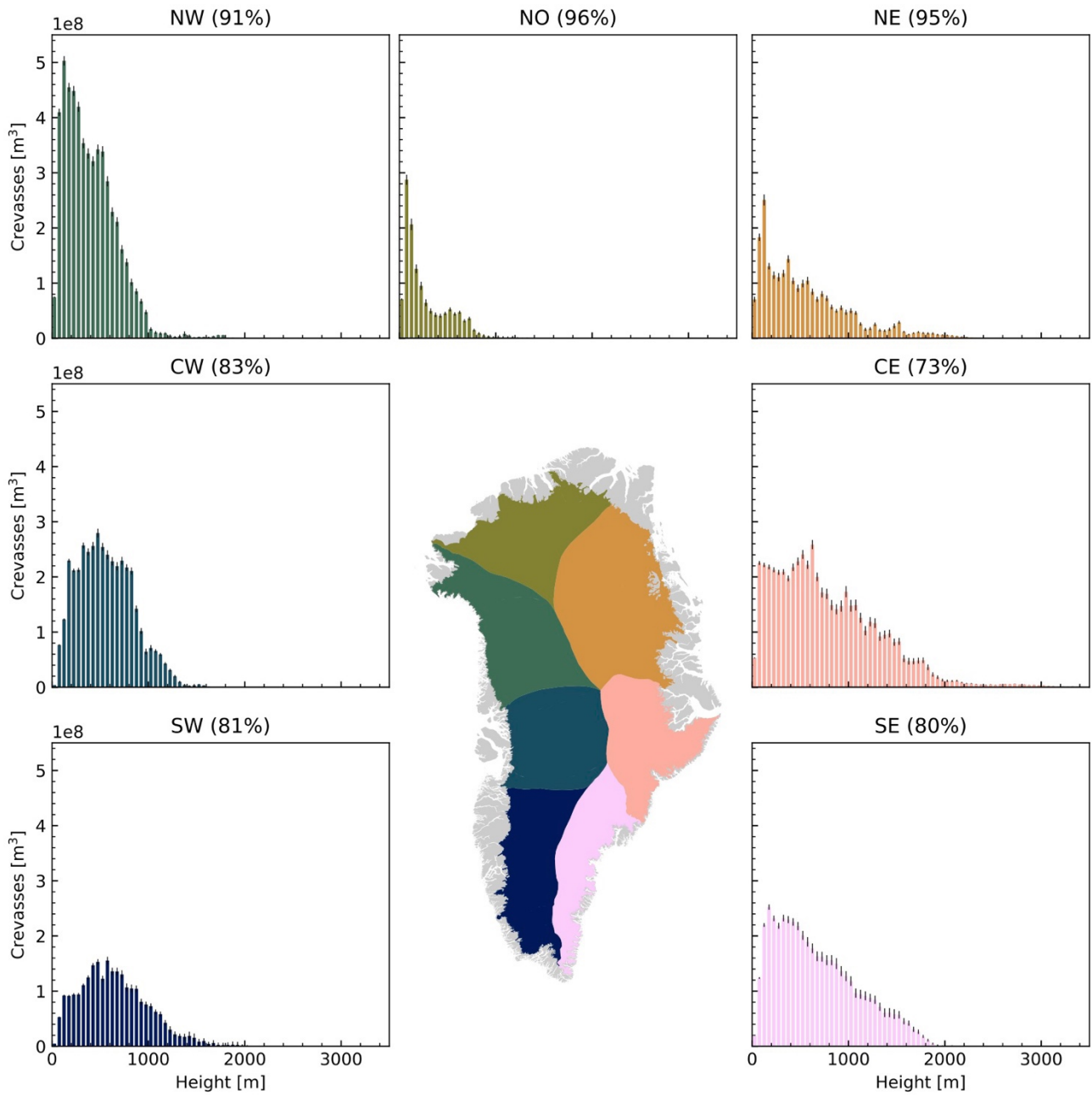
MDK: Formal analysis, investigation, writing – review and editing.

EJM: Methodology, formal analysis, writing – review & editing.

Ethics declaration

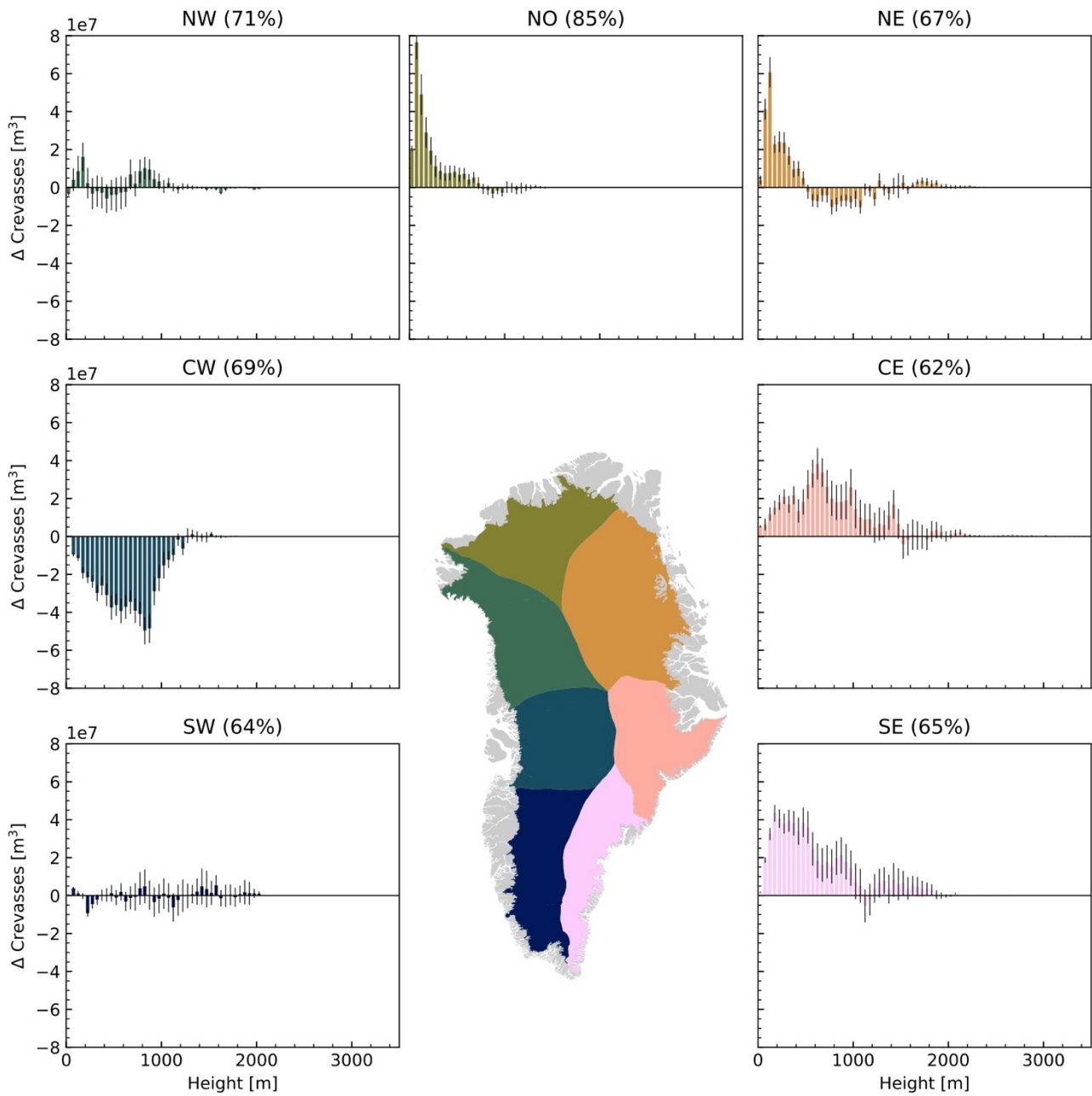The authors declare no competing interests.

635 **Extended Data**

Extended Data Fig. 1*: **Histograms of sectoral crevasse volume in 2021 by surface elevation**.*
Error bars represent 2σ uncertainty. Percentages in figure headings represent proportional data
640 *coverage of sector.*

Extended Data Fig. 2: *Histograms of sectoral crevasse volume change between 2016-2021 by surface elevation*. Error bars represent 2σ uncertainty. Percentages in figure headings

645   represent proportional data coverage of sector.

650 ***Extended Data Table 1: Sectoral and total crevasse volumes for 2021.*** *Discharge represents 2017-2021 average.*

Total Sector Area

Sector	SW	CW	NW	NO	NE	CE	SE	Total
Total Area (km²)	83825	46784	48140	50103	82405	32150	54442	397849

2021 Coverage

Sector	SW	CW	NW	NO	NE	CE	SE	Total
Percentage Cover	81%	83%	91%	96%	95%	73%	80%	86%
Volume (m³)	2.52+E09	4.13+E09	5.42+E09	1.28+E09	2.42+E09	5.55+E09	4.66+E09	25.98+E09
Uncertainty (2σ, m³)	1.92+E08	1.33+E08	1.76+E08	0.97+E08	1.72+E08	2.81+E08	2.53+E08	1.30+E09

655

2016 Coverage

Sector	SW	CW	NW	NO	NE	CE	SE	Total
Percentage Cover	81%	81%	76%	86%	67%	69%	68%	75%
Volume (m³)	2.77+E09	4.54+E09	5.38+E09	1.04+E09	1.82+E09	4.97+E09	3.55+E09	24.06+E09
Uncertainty (2σ, m³)	2.11+E08	1.32+E08	1.48+E08	0.73+E08	1.14+E08	2.41+E08	2.05+E08	1.12+E09

660 **2016 – 2021 Change**

Sector	SW	CW	NW	NO	NE	CE	SE	Total
Percentage Cover	64%	69%	71%	85%	67%	62%	65%	68%
2016 Overlapping Volume (m³)	2.12+E09	4.43+E09	4.65+E09	1.00+E09	1.79+E09	4.59+E09	3.30+E09	21.89+E09
2016 Uncertainty (2σ, m³)	1.53+E08	1.24+E08	1.32+E08	0.71+E08	1.10+E08	2.18+E08	1.95+E08	1.00E+09
2021 Overlapping Volume (m³)	2.13+E09	3.81+E09	4.70+E09	1.26+E09	1.93+E09	5.11+E09	3.90+E09	22.82+E09
2021 Uncertainty (2σ, m³)	1.61+E08	1.17+E08	1.40+E08	0.90+E08	1.19+E08	2.45+E08	2.09+E08	1.09+E09
Difference Volume (m³)	0.04+E08	-6.30 +E08	0.39+E08	2.53+E08	1.48+E08	5.19+E08	6.00+E08	9.32+E08
Difference Uncertainty (2σ, m³)	2.20+E08	1.40+E08	1.58+E08	1.01+E08	1.43+E08	2.81+E08	2.58+E08	13.01+E08
Difference Volume (%)	0.2	-14.2	0.8	25.3	8.3	11.3	18.2	4.3
Difference Uncertainty (%)	10.4	3.2	3.4	10.1	8.0	6.1	7.8	5.9
Significant	N	Y	N	Y	Y	Y	Y	N